

Directivity Investigation of two Annular Phased Array Transducers

Georgios LIAPTSIS¹, Dimosthenis LIAPTSIS², Peter CHARLTON¹

¹Faculty of Applied Design and Engineering, University of Wales Trinity Saint David, Swansea, U.K. Phone: +44(0)1792 481000, e-mail: geoliap@yahoo.com, dimos.liaptsis@twi.co.uk, peter.charlton@sm.uwtsd.ac.uk

²TWI Technology Centre (Wales), Port Talbot, U.K. Phone: 01639873100

Abstract

Annular phased array transducers are well known in the medical field, with their main use being in ophthalmology and dermatology, and have started to be employed in the NDT industry relatively recently. Annular arrays consist of a centre circular element and multiple ring-shaped elements of different width. This unique geometry of the probe makes it difficult to determine the generating beam of the probe. For this reason, it was decided to produce directivity plots for individual elements for both probe configurations. The directivity plots were produced both experimentally and computationally. The generating knowledge of these plots will be novel for annular arrays since no previous work has been reported in the NDT industry.

Keywords: Ultrasonic Testing (UT), Annular Phased Array Transducers, Directivity Investigation, Ultrasonic Beam Profile, Ultrasonic Modelling

1. Introduction

As a continuation of two previous papers ([2] [3]), it was thought to be necessary to investigate the beam directivity of annular phased array transducers. As discussed previously, annular probes are not used as widely as linear array probes because of some inherent limitations. Despite this, annular probes have a lot of unique characteristics which make them superior for some applications. Annular arrays have unique geometry and they can focus in great depths into a material with both a symmetric and circular focal point [1]. It is due to this lack of knowledge that this investigation has been undertaken.

2. Overall Methodology and Results

2.1 Objectives

The directivity plots have fulfilled the following objectives:

- Generate beam profiles for individual elements, both experimentally and computationally.
- Create the opportunity to validate the modelling software.
- Valuable information about the beam characteristics can be extracted from the data analysis of the results, such as natural focal spot size, focal length size and near field for each element.
- Validate the novel near field equation which uses the element area instead of the element outer diameter [2].

2.2 Methodology

In order to plot the beam profile for a particular depth, a known reflector is required. It was decided to use a rod with a stainless steel ball bearing on the top, which can be positioned vertically into the water. In this way, a beam profile is generated without any destructive interference in the index point which potentially exists if two mediums are used. The rod

(which is demonstrated in Figure 1) is made of stainless steel, it is 100mm long and on the top it has a 3mm diameter stainless steel ball bearing.



Figure 1. Stainless steel rod

The inspection parameters used for the experimental work are demonstrated in Table 1.

Table 1. Experimental parameters

	2.5 MHz Probe	5 MHz Probe
Water path (mm)	159	163
Gain (dB)	30	32
Scan area (mm)	30x30	30x30
Index (mm)	0.25	0.25

The same inspection parameters (except the gain) were also used in Civa where a 3mm diameter sphere is placed into water. Furthermore, the probe specifications that are used in Civa were obtained from the probe certificates. The summarised simulation parameters are demonstrated in Table 2.

Table 2. Simulation parameters

	2.5 MHz Probe	5 MHz Probe
Center frequency (MHz)	2.39	4.4
Low frequency (MHz)	1.41	2.73
High frequency (MHz)	3.37	6.78
Bandwidth at -6dB (%)	81.6	76
Number of points	512	512

Each time, a single element is used for both transmission and reception. For the experimental work, the rod was placed into water and an encoded data was collected by scanning an area above the rod. It was decided to scan an area of 30mm x 30mm in order to make sure that the full beam profile is captured. All the measurements were obtained with the same gain for each probe configuration. Also, the data was collected by a really fine scanning increment of 0.25mm in order to have high quality images. After the acquisition of the data, the B-scan values which consisted of multiple A-scans were combined together. The maximum value of each column was extracted and normalised in order to plot the beam profiles. Moreover, the C-scan images for each element were also extracted from the software.

The computational work followed the same trend as the experimental work. The equivalent data analysis occurred in order to create the beam profile for each element and the C-scan images were extracted. Furthermore, some additional data can be extracted from Civa. A very useful tool of the software is the beam computation tool which allows running simulation scenarios and plotting the beam propagation into a medium without the need of a reflector. From this tool, valuable knowledge can be extracted such as the beam propagation images and the on-axis beam propagation plots for two directions, depth and width. Especially from the on-axis plots, valuable quantitative values can be extracted such as near field, focal spot size and focal length size.

The quantitative values were obtained from the on-axis beam propagation plot (z-axis) and from the beam profile plot (x-axis). Figure 2 and Figure 3 demonstrate the methodology that was used to obtain these values. As an example, graphs from element 4 of the 2.5MHz probe are used. The end of the near field is considered the point of the highest energy. The focal beam length and spot are obtained for both -3dB and -6dB drop as figures below illustrate.

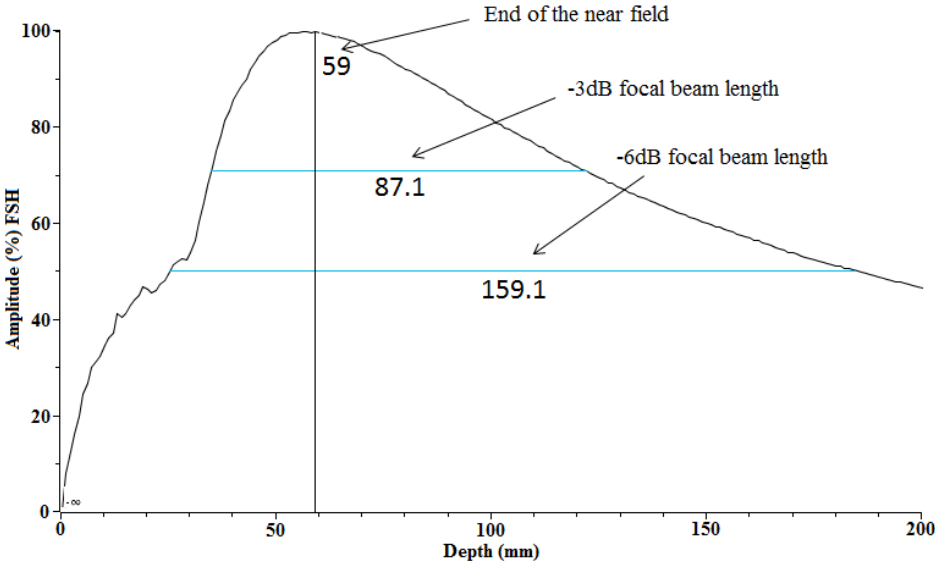


Figure 2. Methodology used to obtain near field and focal length values

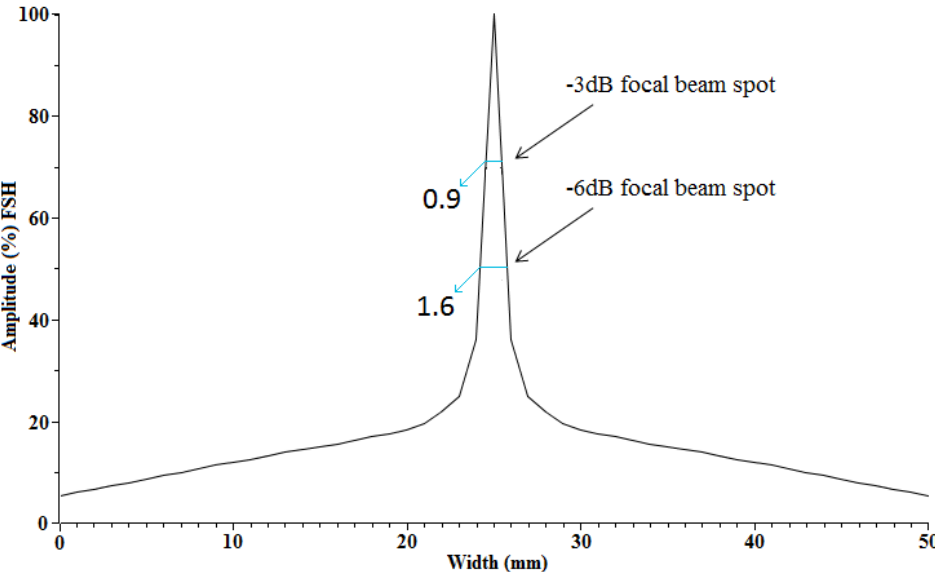


Figure 3. Methodology used to obtain focal spot values

2.3 Results

The beam profiles for each element for both configurations were plotted in a same graph in order to demonstrate the comparison between the experimental and computational results. Some representative graphs, which will help the discussion later, are presented below. Furthermore, the C-scan images are also presented below. Furthermore, from the beam computation tool of Civa, the beam propagation profiles were extracted and presented below as well as the on-axis beam propagation plots for some of the elements.

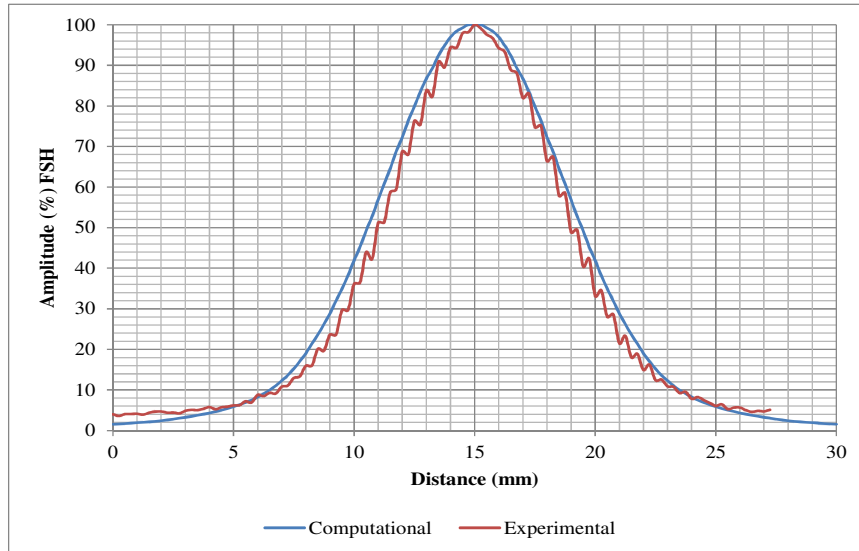


Figure 4. Beam profile comparison for Element 1 of 2.5MHz probe

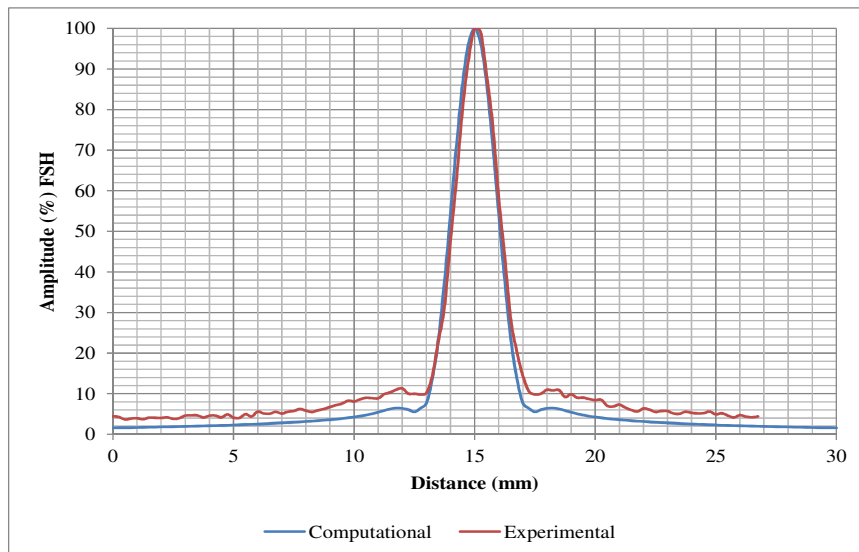


Figure 5. Beam profile comparison for Element 7 of 2.5MHz probe

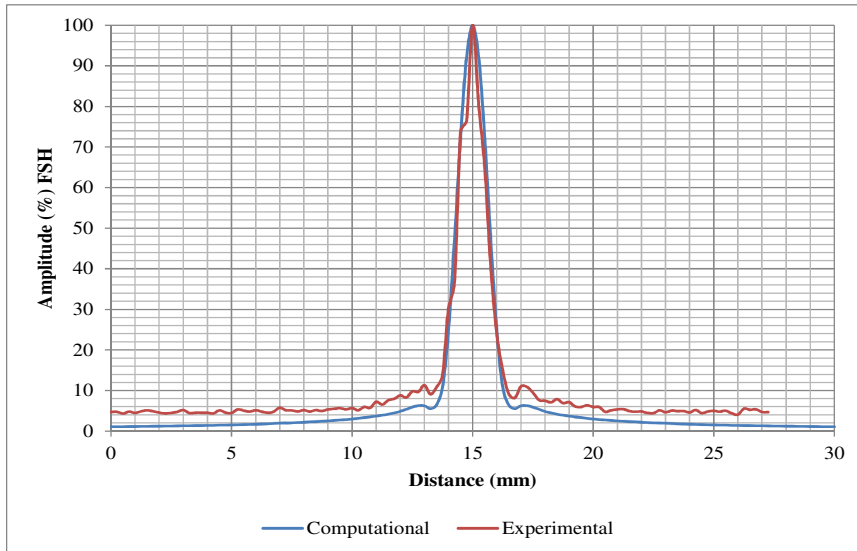


Figure 6. Beam profile comparison for Element 14 of 2.5MHz probe

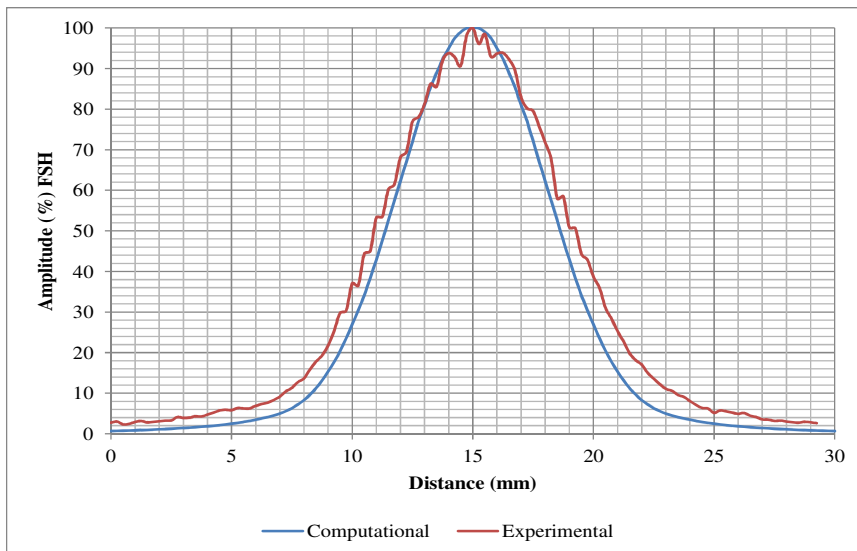


Figure 7. Beam profile comparison for Element 1 of 5MHz probe

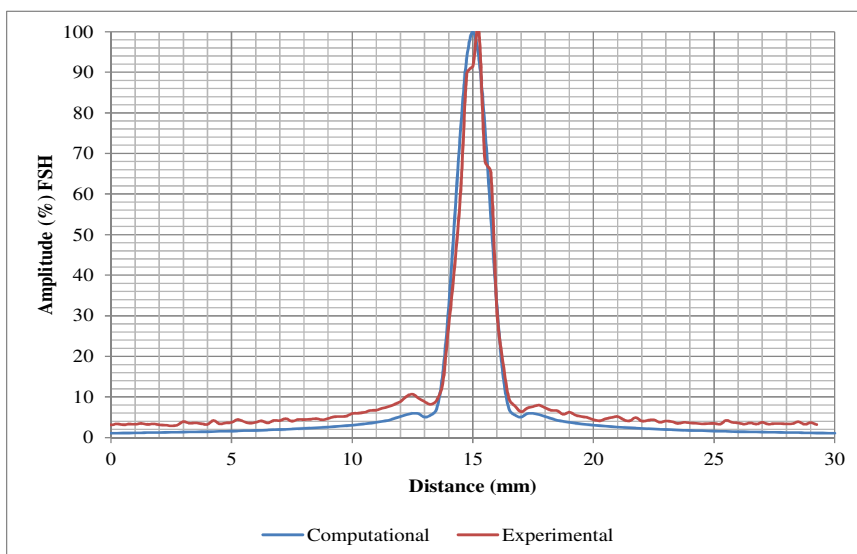


Figure 8. Beam profile comparison for Element 8 of 5MHz probe

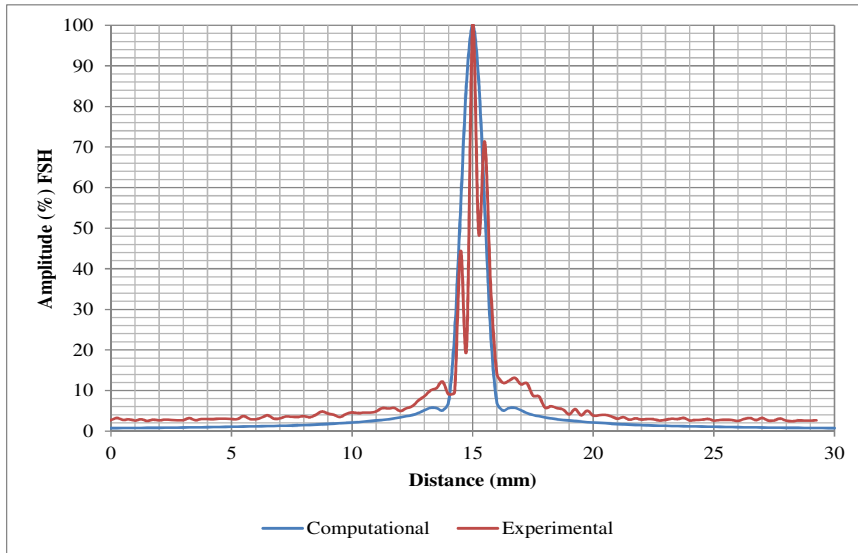


Figure 9. Beam profile comparison for Element 16 of 5MHz probe

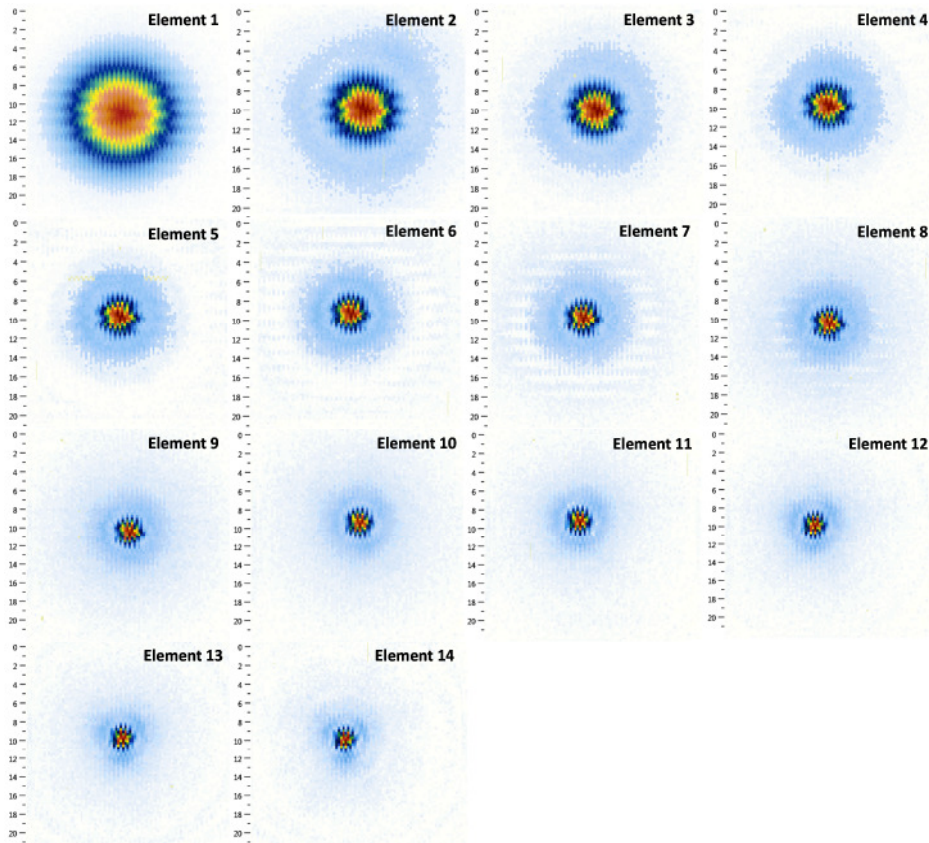


Figure 10. C-scan images of each element for 2.5MHz (experimental)

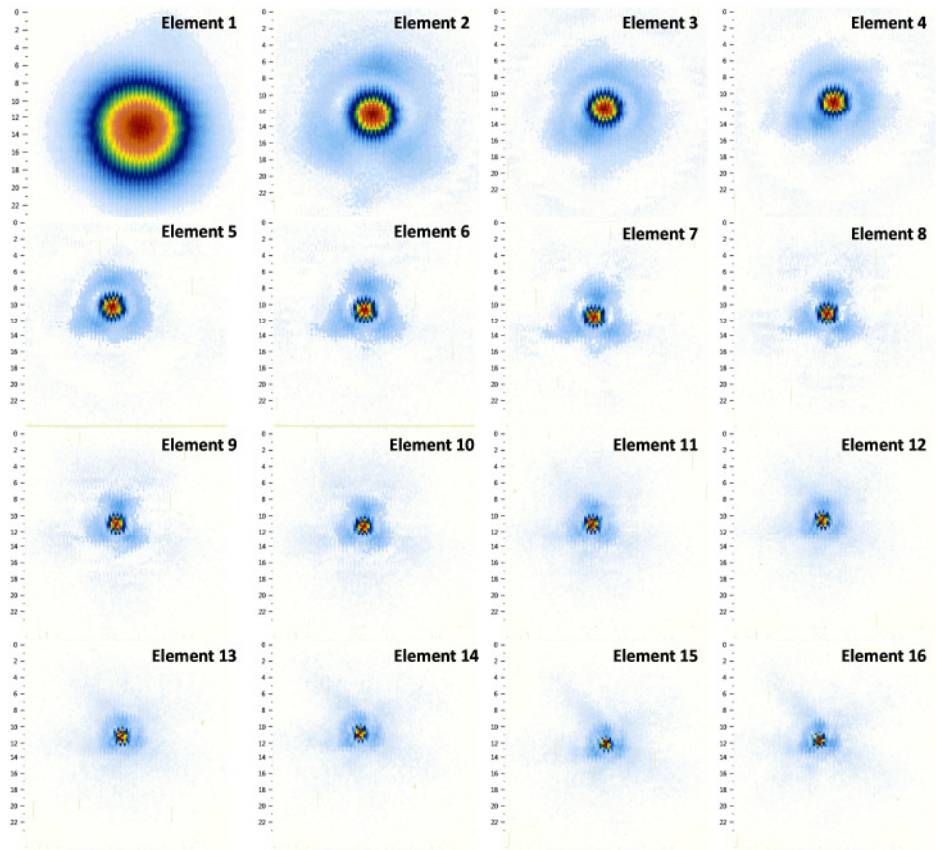


Figure 11. C-scan images of each element for 5MHz (experimental)

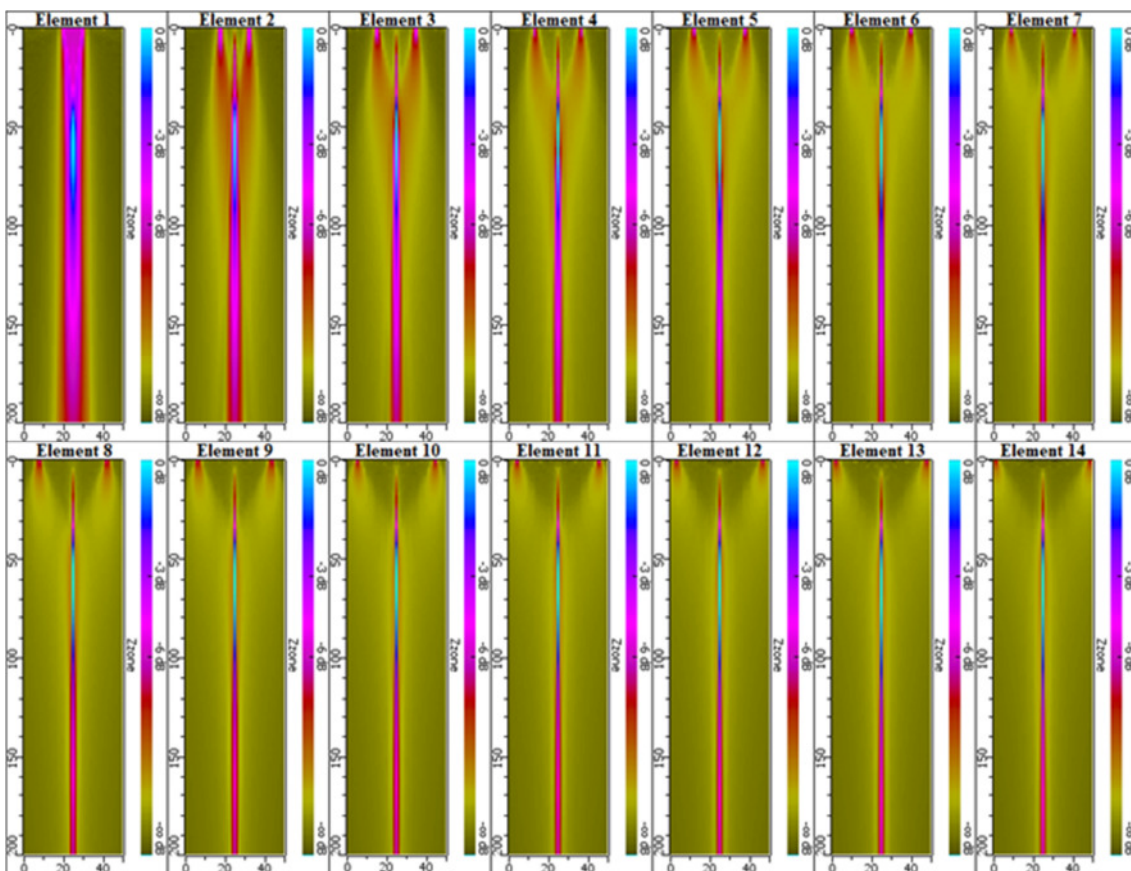


Figure 12. Beam propagation profiles of each element for 2.5MHz probe

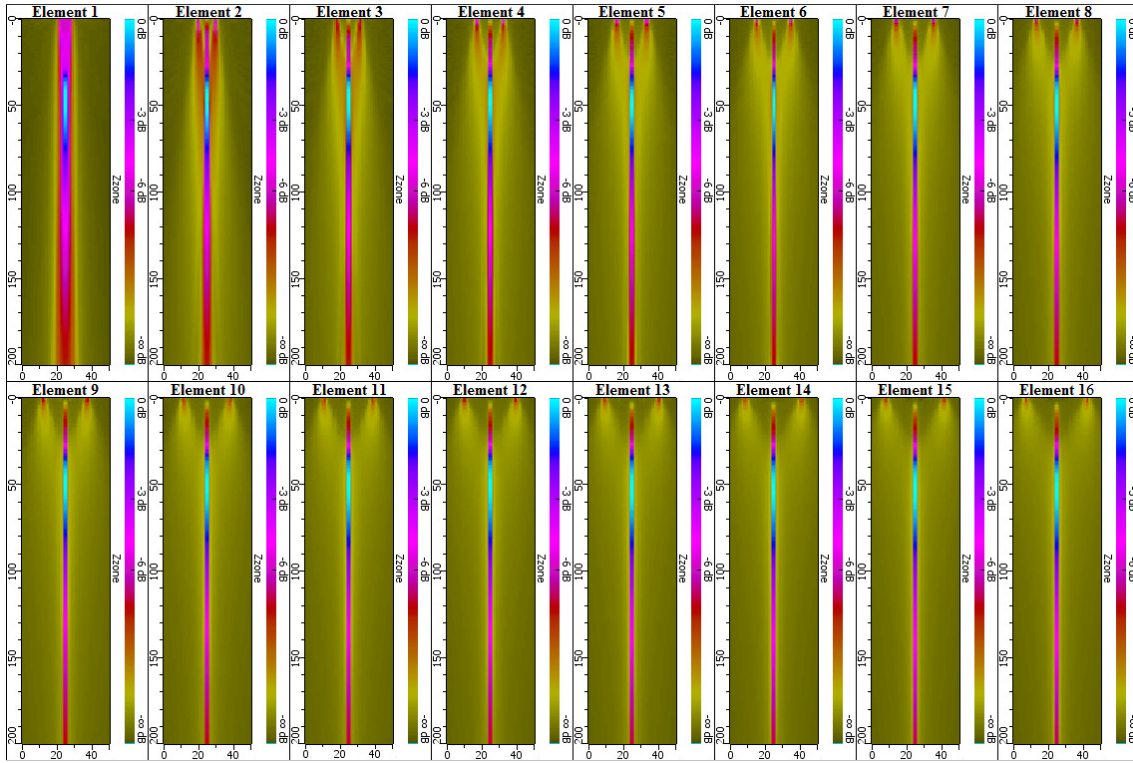


Figure 13. Beam propagation profiles of each element for 5MHz probe

Table 3. Near field and focal length-spot size values for 2.5MHz probe

	dB	Focal spot (mm)	Focal length (mm)	Near field (mm)
Element 1	-3	3.7	82	57
	-6	6.6	177.6	
Element 2	-3	1.8	81.3	58
	-6	2.8	161.9	
Element 3	-3	1.1	85.4	57
	-6	1.9	155.7	
Element 4	-3	0.9	87.1	59
	-6	1.6	159.1	
Element 5	-3	0.8	90	61
	-6	1.4	161	
Element 6	-3	0.8	88.7	59
	-6	1.3	157.8	
Element 7	-3	0.8	89.1	60
	-6	1.3	161.6	
Element 8	-3	0.8	92.4	59
	-6	1.3	162.7	
Element 9	-3	0.8	92.4	58
	-6	1.3	164.5	
Element 10	-3	0.8	93.1	61
	-6	1.3	166.3	
Element 11	-3	0.8	95.5	61
	-6	1.3	170.1	
Element 12	-3	0.8	98.5	62
	-6	1.3	171.6	
Element 13	-3	0.8	102.9	64
	-6	1.3	173.1	
Element 14	-3	0.8	100.1	65
	-6	1.3	174.7	

Table 4. Near field and focal length-spot size values for 5MHz probe

	dB	Focal spot (mm)	Focal length (mm)	Near field (mm)
Element 1	-3	2.5	66.3	46
	-6	4.3	144.1	
Element 2	-3	0.9	67.6	47
	-6	1.6	133.6	
Element 3	-3	0.8	67.5	46
	-6	1.3	127.1	
Element 4	-3	0.8	68.8	47
	-6	1.3	124.1	
Element 5	-3	0.8	69.7	49
	-6	1.3	125.9	
Element 6	-3	0.8	71.4	49
	-6	1.3	127.3	
Element 7	-3	0.8	71.8	45
	-6	1.3	130.8	
Element 8	-3	0.8	73.7	48
	-6	1.3	132.7	
Element 9	-3	0.7	72.7	49
	-6	1.3	130.8	
Element 10	-3	0.7	75.5	49
	-6	1.3	134.1	
Element 11	-3	0.7	77	50
	-6	1.3	137.8	
Element 12	-3	0.7	78.3	49
	-6	1.2	137.1	
Element 13	-3	0.7	79.8	52
	-6	1.2	141.2	
Element 14	-3	0.7	80.6	54
	-6	1.2	141.5	
Element 15	-3	0.7	79.9	51
	-6	1.2	143.1	
Element 16	-3	0.7	80.7	51
	-6	1.2	143.2	

3. Discussion

Figure 4 shows the beam profile of element 1 of the 2.5MHz probe. This element is a circular disk and it seems to have a significant beam spread. Indeed, the reflection from the ball bearing is quite spread out in the time base. The correlation between experimental and computational plots is not exact but it is considered very close. The differences between the two are thought to be due to the actual probes having more broadband response when compared to the simulation input. Furthermore, this is combined with the pulser-receiver characteristics which also contribute to these differences in the beam profile. The experimental plot seems to be a little wavy which was unexpected but it is considered as an artefact of the inspection system.

Figure 5 shows the beam profile of element 7 and demonstrates a tight focused beam as seen in the plot. This result can be explained since as element 7 just like all the elements (except element 1) are rings. As the beam is propagating from the circumference of the virtual circle (ring) it spreads out from the circle but also it tends to focused in the middle. This is why the response from the reflector is focused. Figure 6 shows the beam profile of element 14 (outer element) which is even more focused from element 7. The correlation between computational and experimental plots is very good, almost exact, for both element 7 and 14. It seems that as the diameter of the ring is increased, the beam response seems to be more focused. But as the diameter of the ring is increased, the width of the element is decreased (equal-area). This

generates the question of what parameter is the one which mostly affects the beam. This question is best to be answered in a later section in order to compare all the data (focal length, spot size, near field) and assist to derive reliable conclusions.

The elements of the 5MHz probe follow the same trend. As expected the spread of the centre element is quite large (see Figure 7) and the beam spread rapidly decreased for element 8 and 16 (outer element) as Figure 8 and Figure 9 illustrated. The correlation between computational and experimental plots is good for the centre element and almost exact for element 8 and 16. In Figure 9, some spikes appeared in the experimental plot but it does not affect the defined envelope of the beam profile. It is believed that these spikes are a temporary malfunction which possibly occurred during the acquisition of experimental data (even a loss of a single A-scan can cause a spike).

All the results can be presented in a qualitative form, which allowed a quick comparison of the response from the reflector. Figure 10 and Figure 11 demonstrate the C-scan images of experimental work. The experimental C-scan images suffer from a phenomenon which is called hysteresis which is caused by the software and at the moment of the acquisition of the data could not be eliminated. For this reason the images do not look as good but their quality is sufficient for discussion. The beam spread seems to be larger in 2.5MHz than the 5MHz. This is obvious from the aforementioned figures for all the elements. That was expected since a single element of the 2.5MHz probe has more than twice the area of an element of 5MHz probe. Furthermore, the experimental results have shown higher side lobes which are displayed in the pictures as a light blue spread outside the main response which are not present in the computational images. This is because in computational images the side lobes are below 5% of the main response and in the experimental results are more than 10%. The threshold gate that was used was 10% which explains this phenomenon. Despite the cause of the side lobes, there is a good correlation between the C-scan data.

All the results support the accuracy of the simulation software (Civa) in a non-widely used type of transducers of annular arrays. The validation of the software was proved very useful because valuable results were extracted by running different simulation scenarios instead of running experiments (which takes more time). Therefore a lot of time was saved by this validation.

Figure 12 and Figure 13 demonstrate the 2D beam propagation profiles for each individual element for 2.5MHz and 5MHz probes, respectively. As it was mentioned previously, the images were obtained from Civa and particularly from the beam computation tool. What is advantageous with this tool is that it simulates the beam propagation without the need of a reflector. Each image consisted of an on-axis beam propagation plot (see Figure 2) in z-axis (length of the beam) and multiple beam profile plots (see Figure 3) in x-axis (width of the beam). The software combines together all the values of the aforementioned plots and generates an image which is consisted of different colours. Each colour represents different dB values which are correlated with the amount of energy at each point. The final qualitative result allows having, as close as possible to the reality, the propagation of an ultrasonic beam into a medium. It is worth mentioning that the images of Figure 12 and Figure 13 illustrate the beam propagation into water.

The 2.5MHz probe consisted of 14 elements, so in Figure 12 equal number of beam propagation images are presented. At the exit point of the beam it is possible to see which element is fired and what is the diameter. For example, it is obvious that element 1 is a disc

and element 2 is a ring. Also it is obvious that the width of element 2 is larger than element 14. Furthermore, despite of the element used, the beam is generated in the middle and under the probe surface with small variations as the diameter is increased. Moreover, as the diameter is increased, the element width is decreasing creating a beam, which is nicely focused in the middle. But what is even more surprising is that the natural focus of each element is at the same point. Regardless the element width, and even for element 1 which is a disc, the natural focus point remains the same. This supports the initial theory of the same near field of the elements since they have the same area despite the element shape and diameter. This can be proved by using the quantitative results on the last discussion section.

Other than that, the beam profile seems to become narrower exponentially and not linearly as the element diameter is increased. The beam of the centre element (disc) is very wide, the beam of element 2 is almost 50% narrower, from element 3 pretty much 20% and the differences are becoming smaller until they become negligible. This phenomenon occurs in both probe configurations but in 5MHz probe seems to drop more rapidly. Finally, it is noteworthy that the beam spot sizes of the directivity plots can be obtained by extracting the values of the water path that is used in the experiment and the modelling. The data presented demonstrated the validity of the modelling software compared against the experimental data.

The correlation between the calculated near field values and the measured values has been demonstrated in previous paper [2]. The focal spot sizes for each element are also presented in Table 3 and

Table 4 for both -3dB and -6dB. For the elements of 2.5MHz probe, element 1 (disc) has -3dB focal spot size of 3.7mm and element 2 has 1.8mm (52% drop). The drop between elements 2 and 3 is 39%, between 3 and 4 is 19% and between 4 and 5 is 11%. The focal beam spot size for elements 6 until 14 is the same. Probably, there must be a very small difference which is in scale below 0.1mm (which is the resolution of the modelling).

For the elements of 5MHz probe the drop differences between the focal spot sizes are steeper. The drop between elements 1 and 2 is 64%, between 2 and 3 is 11% and after that remains pretty much the same. This phenomenon must be correlated with the element width. The 5MHz probe is smaller and has more elements therefore the element width decreased rapidly for the inner elements and the differences are minimised for the outer elements. The 2.5MHz probe follows the same tendency but a lot smoother. Hence focal spot size is decreased as the element width decreased and diameter increased.

The focal length values are also presented in the aforementioned tables. The overall differences of the focal lengths are from 82mm to 100.1mm for 2.5MHz probe and from 66.3mm to 80.7mm for 5MHz probe. It seems that the focal length was affected from a different factor than the focal spot since smoother differences occurred. It seems that the focal length increased as the diameter of the element increased but not always, since there are some values which do not follow this trend. A reasonable explanation for this is that it is only affected from the difference between the times of flight between the elements. For example, the beam needs more time to travel in element 14 than element 1.

4. Conclusions

In order to understand how the beam propagates in annular arrays, directivity investigation for individual elements has been carried out both experimentally and computationally. Valuable information has been obtained which leads to the following conclusions:

- Each element of the probe has natural focus at the same point regardless the diameter and the width of each element since the probes use the equal-area manufacturing technique. Additionally, for ring shaped elements, the natural focal point size is decreasing as the element diameter is increasing and width decreasing.
- Very good correlation between computational and experimental beam profiles was achieved and has successfully validated the modelling software.
- The on-axis beam propagation plots have generated many quantitative results. The near field values have been extracted which have been validated against the near field values using the novel equation for individual elements.

Acknowledgements

The authors would like to acknowledge the financial support of the Access to Masters (ATM) scheme.

References

1. Bjorn A.J Angelsen, Hans Torp, Sverre Holm, Kjell Kristoffersen, T.A Whittingham (1995), Which transducer array is best? [Online]. January 1995. Available from: heim.ifi.uio.no/~sverre/papers/95_EurJUS.pdf [Accessed: 29/07/14]
2. Georgios Liaptsis, Dimosthenis Liaptsis, Peter Charlton (2014), Demonstration of a Novel Equation for the Near Field Distance Calculation for Annular Phased Array Transducers [Online]. November 2014. Available from: http://www.ndt.net/article/ndtnet/2014/95_Charlton.pdf [Accessed: 14/11/14]
3. Georgios Liaptsis, Dimosthenis Liaptsis, Ben Wright, Peter Charlton (2015), Focal Law Calculations for Annular Phased Array Transducers [Online]. February 2015. Available from: http://www.ndt.net/article/ndtnet/2015/100_Charlton.pdf [Accessed: 24/02/15]